Predicting the Impact of Dialyzer Choice and Binder Dialysate Flow Rate on Bilirubin Removal

Abstract:

Liver failure is the 12th leading cause of death worldwide. Protein bound toxins such as bilirubin are responsible for many complications of the disease. Binder dialysis systems use albumin dialysate and detoxifying sorbent columns to remove these toxins. Systems like the Molecular Adsorbent Recirculating System (MARS) and BioLogic-DT have existed since the 1990s, but survival benefit in randomized controlled trials have not been consistent. Thus, a new generation of binder dialysis systems, including Open Albumin Dialysis (OPAL) and the Advanced Multi-Organ Replacement System (AMOR) are being developed. Optimal conditions for binder dialysis have not been established. We developed and validated a computational model of bound solute dialysis using established thermodynamic theories. Our objective is to improve AMOR therapy. We confirmed our model's validity by predicting the impact of changing between two benchtop dialysis setups using different polysulfone dialyzers (F3 and F6HPS). We then applied it to predict the impact of varying dialysate flow rate on toxin removal. We found that bilirubin removal is independent of dialysate flow rate within the clinically relevant range (20 mL/min – 800 mL/min), matching our model's predictions. At very low dialysate flow rates (2 mL/min), bilirubin removal declines, deviating from the thermodynamic model. This model may be useful to achieving optimal clinical outcomes by setting optimal dialyzer and flow rate conditions. Further improvement is possible by accounting for toxin adsorption onto the dialyzer membrane.

1 Introduction

In 2021, Liver Failure was the 12th leading cause of death globally (1). The liver performs a variety of critical functions, including toxin removal, drug and food metabolism, protein synthesis including synthesis of clotting factors and immunoproteins, nutrient storage, and other functions. The buildup of toxins during liver failure drives hepatic coma, liver cell death, and failure of other organ systems. Bilirubin is a commonly studied hepatic toxin. Bilirubin accumulation is visible in the skin as jaundice. Excess bilirubin contributes to the pathology of liver failure, for example by damaging white matter (2), which may contribute to hepatic coma. It is also a commonly accepted marker for other albumin-bound toxins.

Bilirubin cannot be removed by traditional dialysis because it is a hydrophobic molecule that is bound to albumin in human blood (3). Adding a binder such as albumin or charcoal to the dialysate allows bilirubin removal (4). Computational modeling of albumin dialysis was first done in the seminal work of Patzer and colleagues, who described single pass albumin dialysis (SPAD) in three publications (4–6). Today, the only FDA approved albumin dialysis system is the Molecular Adsorbent Recirculating System (MARS) (7), which recirculates albumin instead of discarding it after a single pass. Four groups have published models of closed loop mode albumin dialysis.

The first is by Magosso and colleagues (8). This model was designed using clinical data to model MARS sessions. It accounts for ultrafiltration and diffusion. However, it assumes that the dialyzer blood and dialysate compartments and charcoal and resin columns of MARS are well mixed compartments, without modeling concentration gradients. The model has not been validated against data beyond what was used to fit its parameters.

The second is by Annesini and colleagues (9–11). This model applies chemical engineering techniques. Unfortunately, it cannot be applied to bilirubin because it assumes albumin concentration is far greater than toxin concentration. As shown in Table 1, this is not always the case for hyperbilirubinemia in liver failure.

Substance	Molecular Weight (Da)	Average Concentration in Liver Failure (g/L)	Average Concentration in Liver Failure (µM)
Human Serum Albumin	66,438 (12)	9.6 - 56.2 (13)	144 - 846
Bilirubin	584.7 (14)	0.00111 - 0.473	1.9 - 809.8 (13)

Table 1: Albumin and bilirubin concentrations in liver failure can be of the same order of magnitude. Values are minima and maxima.

The third is by Pei and colleagues, who extended the work of Patzer to include recirculation and the effect of local ultrafiltration (15–18). Unfortunately, when we replicated their model, we were unable to reproduce their results. They reported results for three initial blood bilirubin concentrations: 14.7, 17.7 and 21.4 mg/dL. Reported modeled final blood bilirubin concentrations from Pei et al are 7.7, 9.0 and 10.8 mg/dL. In our attempt to reproduce their model with their parameters, we got final bilirubin concentrations of 10.36, 11.08, 11.76 mg/dL.

Their code is not publicly available, and parts of their model, such as the equation for ultrafiltration rate in the Peclet Number formula, are not reported, making it difficult to identify why their data could not be reproduced. In our attempt to replicate the model we used the definition of Peclet Number provided in Villarroel et al (19).

The last effort was by Schiesser (20). This model couples a 2 ordinary differential equation (ODE) patient model with an 8 partial differential equation (PDE) model for the extracorporeal device. It has not been validated against experimental data.

MARS has not shown consistent survival improvements in randomized controlled trials (21,22). Today, a new generation of binder dialysis systems are being developed. These include the Advanced Multi-Organ Replacement System (AMOR) (23), Open Albumin Dialysis (OPAL) (24), and High Efficiency MARS (HE-MARS) (25). Our goal is to optimize AMOR using this algorithm, but any binder dialysis system could be modeled in this way.

2 Methods

2.1 Model Description:

The model was constructed similarly to that of Pei and colleagues (15–18). Blood and dialysate were assumed to be two well-mixed compartments containing albumin and the toxin of interest. Toxin removal was assumed to happen by diffusion and convection across a dialyzer

membrane with blood and dialysate flowing counter-current. The removal of toxin across the dialyzer was solved at each time step by solving a spatial model of concentrations, pressures, and flow rates. This was used to update the blood and dialysate concentrations. The Peclet number was defined following Villarroel et al (19). Unlike the model of Pei and colleagues, a piecewise function was used to account for the change in the sign of convective flux across the dialysis membrane during backfiltration.

2.2 Variable Names:

P_b → blood pressure, P_d → dialysate pressure, z → distance along dialyzer fiber from blood inlet and dialysate outlet. μ_b → viscosity of blood. μ_d → viscosity of dialysate. Q_b → blood flow rate. Q_d → dialysate flow rate. r_i → inner dialysate fiber radius. r_o → outer dialysate fiber radius. R_m → inner radius of dialyzer shell (constrains the dialysate space outside the fibers). n → number of fibers. L_p → Membrane hydraulic permeability. C_{stlb} → total blood bilirubin concentration. C_{stld} → total dialysate bilirubin concentration. C_{sb} → free blood bilirubin concentration. C_{sd} → free dialysate bilirubin concentration. C_{atlb} → total blood albumin. C_{atld} → total dialysate albumin. $K_{free}A$ → a coefficient representing the diffusive transport of unbound bilirubin across the entire area of the dialyzer membrane. K_B → Albumin-bilirubin binding constant, J_v → local ultrafiltration flux. f → function of Peclet Number. σ → reflection coefficient of the membrane. L → dialyzer length. pe → Peclet Number, a dimensionless quantity relating convection and diffusion. V_b → blood reservoir volume. V_d → dialysate reservoir volume.

2.3 Boundary Conditions:

$P_d(z=0)=0$ (dialysate outlet pressure), $C_{stlb}(z=0,t=0)=C_{stlb,in}$ (input blood side bilirubin). $C_{stld}(z=L,t=0)=0$ (dialysate initially has no bilirubin). $Q_b(z=L)=Q_b(z=0)$ (no net ultrafiltration). $Q_d(z=L)=Q_d(z=0)$ (no net ultrafiltration). $Q_b(z=0)=Q_{b,in}$ (blood inlet flow rate). $Q_d(z=L)=Q_{d,in}$ (dialysate inlet flow rate).

2.4 Equations:

Change in blood pressure with respect to z: $\frac{dP_b}{dz}=-\frac{8\mu_b Q_b}{n\pi r_i^4}$ (Eq 1. from eq. 2 in (18))

Change in dialysate pressure with respect to z: $\frac{dP_d}{dz}=\frac{8\mu_d(R_m+nr_o)^2 Q_d}{\pi\left(R_m^2-nr_0^2\right)^3}$ (Eq. 2 from eq. 3 in (18))

Change in blood flow rate with respect to z: $\frac{dQ_b}{dz}=-2n\pi r_i L_p(P_b-P_d)$ (Eq. 3 from eq. 4 and 6 in (18))

Change in dialysate flow rate with respect to z: $\frac{dQ_d}{dz}=-2n\pi r_i L_p(P_b-P_d)$ (Eq. 4 from eq. 5 and 6 in (18))

Change in blood and dialysate total bilirubin concentration multiplied by flow rate with respect to z: This equation is modified from Pei et al's eq. 7 and 8 (18). Unlike the previous model, we account for the change in the direction of convection across the dialyzer membrane when dialysate pressure exceeds blood pressure. A purely diffusive mode is introduced for small values of J_v to avoid division by zero errors when calculating f (see below).

$$\frac{d(Q_b C_{stlb})}{dz} = \frac{d(Q_d C_{stld})}{dz} = \begin{cases} \left(J_v(1-\sigma)f - \frac{K_{free}A}{L}\right) * (C_{sb} - C_{sd}) - J_v(1-\sigma)C_{sb} \; if \; J_v > J_{v,crit} \\ -\frac{K_{free}A}{L} * (C_{sb} - C_{sd}) \; if \; -J_{v,crit} < J_v < J_{v,crit} \\ \left(J_v(1-\sigma)f - \frac{K_{free}A}{L}\right) * (C_{sb} - C_{sd}) - J_v(1-\sigma)C_{sd} \; if \; J_v < -J_{v,crit} \end{cases} \quad \text{(Eq. 5)}$$

$J_{v,crit}$ is calculated by the following criterion:

$$J_{v,crit} = \min(Q_b, Q_d) * 10^{-5} \frac{mm^3}{s} \text{ (Eq. 6)}$$

Blood free bilirubin in terms of blood total bilirubin: $C_{sb} = \frac{-\left(C_{atlb} + \frac{1}{K_B} - C_{stlb}\right) + \sqrt{\left(C_{atlb} + \frac{1}{K_B} - C_{stlb}\right)^2 + \frac{4C_{stlb}}{K_B}}}{2}$ (Eq. 7, from eq. 9a in (18))

Dialysate free bilirubin in terms of dialysate total bilirubin: $C_{sd} = \frac{-\left(C_{atld} + \frac{1}{K_B} - C_{stld}\right) + \sqrt{\left(C_{atld} + \frac{1}{K_B} - C_{stld}\right)^2 + \frac{4C_{stld}}{K_B}}}{2}$ (Eq. 8 from eq. 9b in (18))

$J_v = 2n\pi r_i \, L_p(P_b - P_d)$ (Eq. 9, from local ultrafiltration rate, eq. 6 in (18))

$f = \frac{1}{Pe} - \frac{1}{\exp(Pe) - 1}$ (Eq. 10, from function of Peclet Number given by Pei et al. (18))

The equation for Peclet number is derived from eq. 9 in Villarroel et al. (19)

$$Pe = J_v * (1 - \sigma) * \frac{L}{kA} \text{ (Eq. 11)}$$

As flow rate changes, albumin concentration also changes, but since flow rate is periodic, so is albumin concentration. Thus, it doesn't change over time, only spatially.

$$C_{atlb} * Q_b(z) = C_{atlb}(z = 0) * Q_b(z = 0) \text{ (Eq. 12, from 9b in (18))}$$

$$C_{atld} * Q_d(z) = C_{atld}(z = L) * Q_d(z = L) \text{ (Eq. 13, from 10b in (18))}$$

Time dependence is described as follows:

$$\frac{d\left(C_{stlb,z=0} * V_{br}\right)}{dt} = C_{stlb,(z=L)} * Q_{b,out} - C_{stlb,(z=0)} * Q_{bin} \text{ (Eq. 14, from 11a in (18))}$$

$$\frac{d\left(C_{stld,z=0} * V_{dr}\right)}{dt} = C_{stld,(z=0)} * Q_{d,out} - C_{stld,(z=L)} * Q_{din} \text{ (Eq. 15, from 12a in (18))}$$

Because of numerical instability, a shooting method was used to solve the boundary value problem posed by counter-current flow in the dialyzer. The model was implemented using Julia Version 1.9.3 (26) with the packages Revise.jl, XLSX.jl, DifferentialEquations.jl (27), FileIO, JLD2, ODEInterfaceDiffEq (27), NonlinearSolve (28), NLSolve (29), LinearAlgebra, and Roots (30). We used the Julia function linspace provided by Jonathan Bieler (31). We used the Julia remove function provided by Michael Franco (32). We used the myfind Julia function (33). The radau solver was used for the spatial solution (34). The built-in solver selection algorithm of DifferentialEquations.jl was used for the temporal differential equation solution (35).

Details of the algorithm used to achieve numerical stability in solving this system are available in our provisional patent application (36). Parameter sweeps were conducted on the University of Washington's Hyak Supercomputer. Goodness of fit was analyzed by minimizing the sum of squares (goodness of fit to the entire solution) or by minimizing the percent error at the end of the trial (goodness of fit to the equilibrium bilirubin concentration). The two criteria are shown in Eq. 16 and Eq. 17 respectively. Here, t is time during the trial. t_{end} is the time at the end of the trial. C_{true} is the measured concentration. C_{model} is the concentration predicted by the model. i is an index that varies from 1 to n where n is the number of time points.

$$Error = \sum_{i=1}^{n}\left(C_{model}(t = t_i) - C_{true}(t = t_i)\right)^2$$ Eq. 16 (Sum of Squares Goodness of Fit Criterion)

$$Error = \frac{\left(C_{model}(t=t_{end}) - C_{true}(t=t_{end})\right)*100\%}{C_{true}(t=t_{end})}$$ Eq. 17 (Percent Error Goodness of Fit Criterion)

2.5 Experimental Procedure:

Five sets of experiments were done in total:

- Condition 1: A pilot study (n = 3) using Bovine Serum Albumin (BSA) on both sides of an F6HPS dialyzer (Fresenius, Waltham, MA, USA) with blood and dialysate flow rates of $Q_b = 180$ mL/min and $Q_d = 90$ mL/min. This was used to fit two parameters:
    - 1: The dialyzer diffusive mass transfer coefficient for free bilirubin moving through polysulfone ($K_{free}A$)
    - 2: The bilirubin binding equilibrium constant for the primary binding site on BSA (kB,BSA)
- Condition 2: A validation data set (n = 3) using BSA on both sides of an F3 dialyzer (Fresenius, Waltham, MA, USA) with blood and dialysate flow rates of 150 mL/min
- Condition 3: A test data set (n = 3), like condition 2, but with the dialysate flow rate set to 20 mL/min, as previously described in a pilot study of a novel albumin dialysis system (23)
- Condition 4: A test data set (n = 3), like condition 2, but with the dialysate flow rate set at 800 mL/min, which is the highest flow rate we have found in clinical practice (37)
- Condition 5: A test data set (n = 3), like condition 2, but with the dialysate flow rate set at 2 mL/min, which is relevant in some neonatal dialysis applications (38)

The precise values for the setups are summarized in Table 3. The F6HPS trials (setup 1) was used to set model parameters. These were the toxin binding affinity for albumin, and the dialyzer mass transfer-area coefficient for free bilirubin diffusion ($K_{free}A$). The F3 trials were used to independently validate model predictions. The $K_{free}A$ value was adjusted between the two dialyzers (see Section 2.7). Flow rate was set using Masterflex Pumps with model numbers 07551-20 and 77521-40, using Easy-Load II Rotors with Model Number 772990-62 (Cole-Parmer, East Bunker, CT, USA) except for the 2 mL/min trial, in which an Ismatec 78017-10 (IDEX Corporation, Northbrook, IL, USA) pump was used on the dialysate side. Pressure was controlled using four RSCDRRE015PGSE3 pressure sensors (Honeywell International Inc, Charlotte, NC, USA) to prevent ultrafiltration, except in the 800 mL/min trial, where more robust

PS04-G100KP-A4W pressure sensors (Same Sky, Lake Oswego, OR, USA) were used. Data from Honeywell pressure sensors were obtained using a Raspberry Pi 3B (Raspberry Pi, Cambridge, England, UK). Same Sky pressure sensor readings were processed using an HX711 (Sparkfun, Niwot, CO, USA) connected to an Arduino Uno (Arduino SA, Chiasso, Switzerland). Pressure was adjusted using c-clamps. The blood and dialysate reservoirs were immersed in a 37 °C water bath (Benchmark, Sayreville, NJ), except in Setup 1. There, temperature was measured by K type thermocouples connected to a Measurement Advantage DAQ and maintained near 37 °C on both sides using hotplates. Hotplates were from Corning (Glendale, AZ, USA), with model numbers PC-420, and PC-420D. K-type thermocouples were from MN Measurement Instruments (St. Paul, MN, USA). The DAQ was from Measurement Computing (Norton, MA, USA). Figure 1 shows diagrams of the circuits for each setup.

Solute concentrations, along with references supporting their clinical relevance, are listed in Table 2. pH on the blood and dialysate side was maintained between 7.35 and 7.45 using a pH Meter (OrionStar A211, Thermo Scientific, Waltham, MA), except in Setup 1, where the pH was maintained between 7.2 and 7.5 using the less precise pHoenix XL meter from MesaLabs. For Setup 1, pH in this was initially set at 7.2 ± 0.1 following previous work on protein bound toxin removal by our group (18). Acidosis is common in CKD patients (39,40). However, pH values below 7.3 are unusual. Acknowledging this, we increased the pH set point in later Setup 1 trials to 7.4 ± 0.1. In all setups, pH adjustment was done using 1 N HCl and NaOH. pH was set at 35-40 °C, determined using hotplates and thermocouples as previously described. In all setups care was taken to protect the setup from light to minimize photodegradation of bilirubin. For Setup 1, dialyzers were reused after being cleaned according to established clinical protocols (41,42). Bilirubin and Albumin measurement protocols were the same as in our previous work (23).

Solute	Concentration
BSA	2 g/dL (13)
Bilirubin	20 mg/dL (43,44)
Cholic Acid	19.3 µM (45)
Creatinine	15 mg/dL (46)
Indoxyl Sulfate	4 mg/dL (47)
Copper	21.56 µM (48)
Manganese	2.5 µM (48)

Table 2: Toxin concentrations in blood analog solution.

	Setup 1	Setups 2-5
Duration (hr)	3	5
Blood Analog Solution Volume (mL)	628.33	200
Dialysate Volume (mL)	626.67	200
Blood flow rate (mL/min)	180	150
Dialysate flow rate (mL/min)	90	2, 20, 150, 800
Ultrafiltration rate (mL/min)	0	0
Blood Albumin Concentration (g/dL)	2	2
Dialysate Albumin Concentration (g/dL)	2	2
Blood Albumin	BSA	BSA
Dialysate Albumin	BSA	BSA
Dialyzer	F6HPS	F3
Material	Polysulfone	Polysulfone
Number of Fibers	8400 (49)	2304 (49)
Hollow Fiber Inner Radius (µm)	100 (50)	100 (51)
Hollow Fiber Outer Radius (µm)	140 (50)	140 (52)
Hollow Fiber Length (cm)	21 (53)	20 (51)
Area (m^2)	1.3 (50)	0.4 (51)
Housing Inner Radius (mm)	20 (50)	11 (measured)
Bilirubin Reflection Coefficient (assumed (18))	0	0

Table 3: Albumin Dialysis Setups Used in This Study

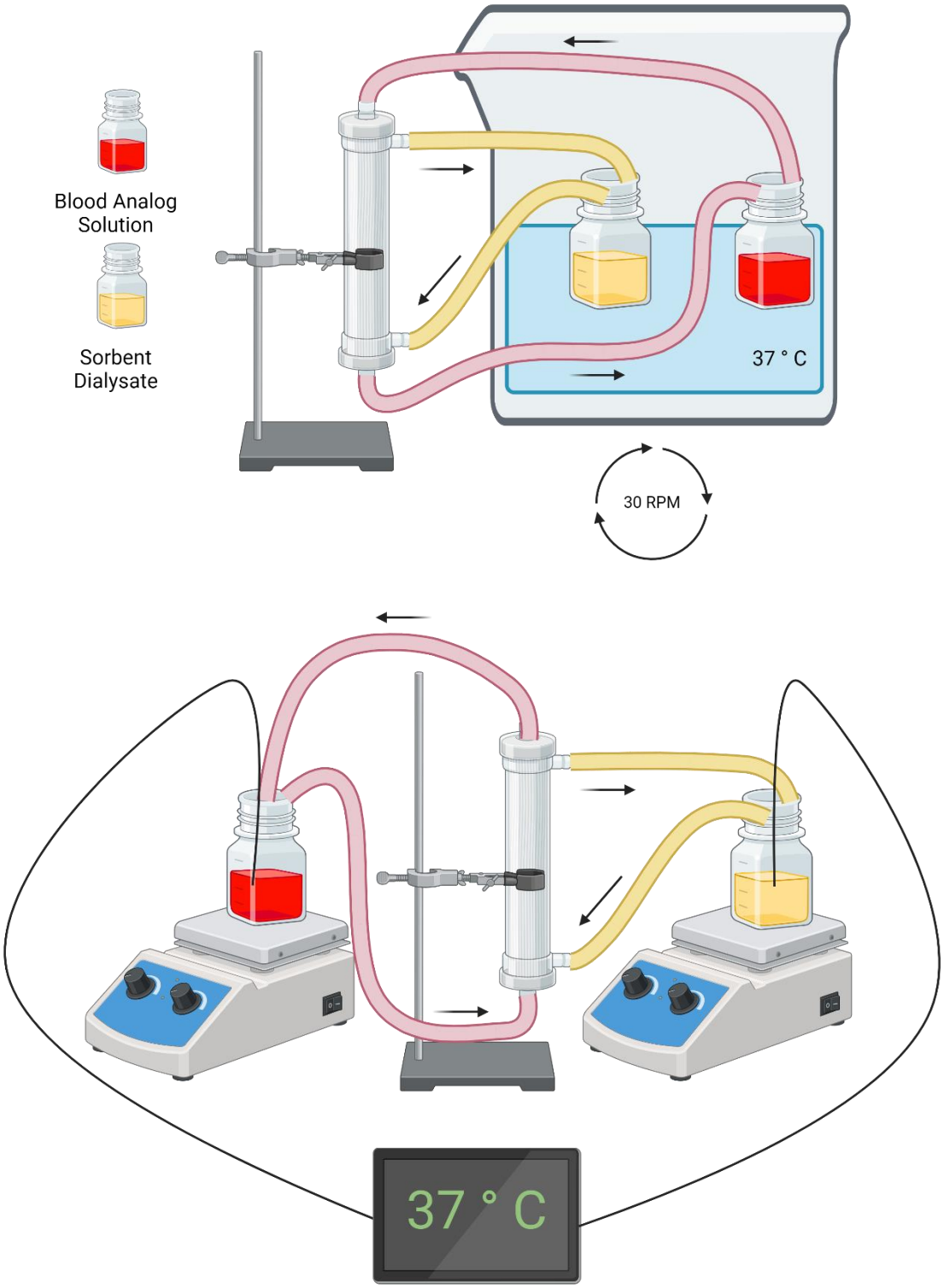

Figure 1: Experimental setup for conditions 2-4 (top) and condition 1 (bottom)

2.6 Polysulfone Membrane Hydraulic Permeability:

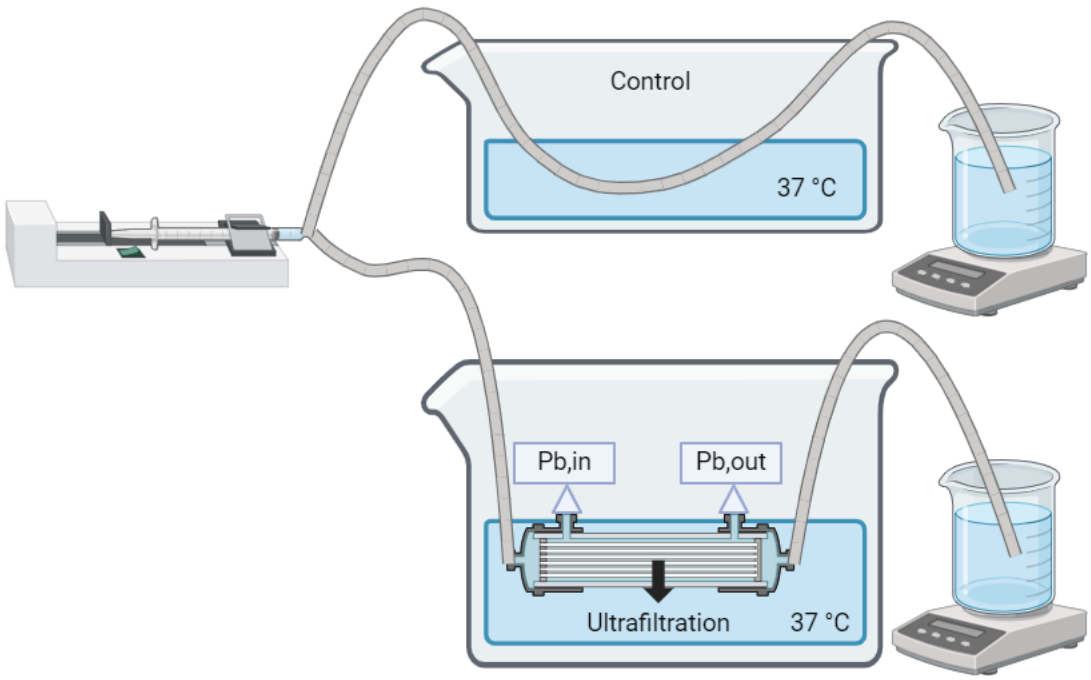

Figure 2: Hydraulic Permeability Test Setup. Figure created with BioRender.

Polysulfone membrane hydraulic permeability was measured by a method based on the work of Liao et al (54), with some modification. A small dialyzer, called a “mini-module” was created out of individual F6HPS dialyzer fibers in a custom-made casing. Figure 2 shows the test setup. The formula for hydraulic permeability was:

$$L_p = \frac{\Delta V/\Delta t}{P*A} \text{ (Eq. 18)}$$

ΔV refers to the ultrafiltration volume. Δt is the time. A is the total area of the dialysis membrane in the mini-module. Here, pressure is calculated as:

$$P = \frac{P_{b,in}+P_{b,out}}{2} - \frac{P_{d,in}+P_{d,out}}{2} \text{ (Eq. 19)}$$

In this formula, $P_{b,in}$ is the inlet blood pressure and $P_{b,out}$ is the outlet blood pressure. $P_{d,in}$ and $P_{d,out}$ are the corresponding dialysate pressures. Since the module is near the surface of a stirred water bath and the dialysate side is in contact with the water (Figure 2), the dialysate pressures are approximately equal and negligible.

Mini-modules were constructed out of F6HPS dialyzer polysulfone fibers. Fibers were carefully selected to be straight, to avoid any damage or kinking. Two mini-modules were constructed (designated F6HPS and F6HPS2). They were then bundled together in a fitting using Gorilla Epoxy (Gorilla Glue, Cincinnati, OH, USA). A neMESYS Low Pressure Syringe

Pump (Cetoni, Korbussen, Germany) was used to set precise flow rates. Pressure on the inlet and outlet of the mini-module was measured using PX409-USBH sensors (Omega Engineering, Norwalk, CT, USA). Mini-modules were immersed in a 37 °C water bath. Heating, stirring, and temperature control was provided using hotplates, K-type thermocouples, and a data acquisition unit (DAQ). Hotplates were from Corning (Glendale, AZ, USA), with model numbers PC-420, and PC-420D. K-type thermocouples were from MN Measurement Instruments (St. Paul, MN, USA). The DAQ was from Measurement Computing (Norton, MA, USA). Flow through the mini-module was compared to flow through a control tube. The difference was the ultrafiltration rate ΔV. Following Liao et al (54), flow rates of 1910 $\frac{\mu L}{min}$, 764 $\frac{\mu L}{min}$, and 191 $\frac{\mu L}{min}$ were tested for both mini-modules. One of the 191 $\frac{\mu L}{min}$ tests was an extreme outlier, so it was repeated, and 382 $\frac{\mu L}{min}$ was also tested for that mini-module. These additional tests did not replicate the outlier value, so the outlier value was then discarded.

2.7 Fit Parameters:

Two parameters were fit computationally rather than being determined from the literature. The first was the primary binding constant for bilirubin-BSA binding. All literature values for this parameter fall within a narrow range (Table 4). The primary binding site of bilirubin on BSA has approximately an order of magnitude greater affinity than the secondary binding site (55). Thus, the secondary binding site was neglected for this analysis. the constant for the primary binding site was fit. The lower bound of the search space was set to 0.5E7 (1/M). The upper bound was set to 7.5E7 (1/M). The space was searched in steps of 1E7 (1/M).

Study	Primary Bilirubin-BSA Binding Constant (1/M)	Temperature (ºC)	Solution	pH
Chen, 1973 (55)	2.2E7	25	0.1 M potassium phosphate buffer	7.4
Faerch and Jacobsen, 1974 (56)	2.7E7	37	67 mM phosphate buffer	7.4
Rubaltelli and Jori, 1979 (57)	2.16E7	19	0.5 M KH2PO4-Na2HPO4 buffer	7.4
Muzaffar et al, 1991 (58)	1.05E7	30	Tris-HCl buffer	8.0
Williams et al, 2002 (59)	1.2E7	Room temperature	0.125 M phosphate buffer	7.4
Chen et al, 2007 (60) by fluorescence enhancement	6.57E7	Not given	Double-distilled water	Not given
Chen et al, 2007 (60) by fluorescence quenching	4.34E7	Not given	Double-distilled water	Not given

Table 4: Reported values of bilirubin-BSA binding constant

The second fit parameter was the product of the dialyzer mass transfer-area coefficient for free bilirubin diffusion and area ($K_{free}A$). The highest value of this coefficient reported in the literature is 2000 mL/min, discussed by Meyer et al (61). Thus, this parameter was optimized over the range from 100 to 2500 mL/min in steps of 100 mL/min. In Equation 5 this coefficient is analogous to KoA for toxins which are not protein bound, but there are important differences. This coefficient does not relate directly to the clearance of the toxin of interest by the standard relationship given in Michaels (62). This calculation assumes that the mean concentration difference in counter-current dialysis is the logarithmic mean of the inlet and outlet concentration differences. For free bilirubin, this is not the case. On the blood side, as free bilirubin crosses the membrane the unbound concentration declines. This creates a thermodynamic driving force for the release of additional bilirubin from albumin. In contrast, on the dialysate side as bilirubin crosses the membrane, it binds to free binding sites on dialysate albumin. This lowers the free dialysate side bilirubin concentration. Additionally, this coefficient depends on the assumption that blood and dialysate side clearance are approximately equal. Other processes such as membrane binding of bilirubin may cause blood side clearance to exceed dialysate side clearance. Polysulfone membranes have been observed to bind small quantities of bilirubin (63). This would lead to an apparently elevated $K_{free}A$ being the best fit parameter because it must account for other processes such as membrane binding.

Afterwards, $K_{free}A$ was adjusted to account for a new dialyzer following equation 20. Because the F3 and F6HPS dialyzers are both polysulfone, it was assumed that area was the only adjustment needed, meaning the two dialyzers had the same value of K_{free}. The dependence of $K_{free}A$ flow rate (64) was neglected.

$$koA_{new} = koA_{old} * \frac{A_{new}}{A_{old}} \text{ (Eq. 20)}$$

3 Results

3.1 Hydraulic Permeability:

Hydraulic permeability was measured as 8.61*10^(-11) m/(s*Pa) $\pm$ 2.14 * 10^(-11) m/(s*Pa) (average $\pm$ standard deviation). This measurement was used for subsequent modeling. This is much lower than the value obtained by Liao et al for polysulfone of 1.628*10^(-9) m/(s*Pa) (54). However, it is comparable to the value obtained by Benavente and Jonsson of 10^(-10) m/(s*Pa) (65). Hydraulic permeability test raw data is reported in Table 5. The discarded outlier test is highlighted in yellow. Averages and standard deviations are reported in Table 6.

Lp (m/s*Pa)	Mini-Module	Flow Rate (uL/min)	$P_{b,in}$ (cm H2O)	$P_{b,out}$ (cm H2O)	Delta V (mL)	Time (min)
1.013E-10	F6HPS2	1910	209.7	3.94	0.628	10.5
1.020E-10	F6HPS2	764	65.139	2.615	0.383	20
9.601E-11	F6HPS2	382	35.828	2.58	0.409	40
2.768E-11	F6HPS2	191	19.76	4.162	0.11	60
8.851E-11	F6HPS2	191	21.127	2.904	0.473	80
9.750E-11	F6HPS	1910	531.57	3.726	1.45	10
7.463E-11	F6HPS	764	269.35	1.955	1.122	20
4.257E-11	F6HPS	191	50.8	4.507	0.522	80

Table 5: Hydraulic Permeability Measurements from Individual Trials. Lp refers to hydraulic permeability. $P_{b,in}$ refers to blood side (luminal) inlet pressure. $P_{b,out}$ refers to blood side outlet pressure. Delta V refers to the change in volume.

Mini-Module	Average Lp (m/s*Pa)	Standard Deviation (m/s*Pa)
F6HPS	7.157E-11	2.75928E-11
F6HPS2	9.696E-11	6.233E-12
Total	8.61E-11	2.14E-11

Table 6: Average and standard deviation hydraulic permeability values for both mini-modules and overall.

3.2 Albumin Dialysis Study

Table 7 summarizes measured average starting bilirubin and albumin concentrations for all five setups. These values were used for modeling to avoid error caused by variations in the initial solution composition.

Condition	Starting Blood Bilirubin (mg/dL)	Starting Blood Albumin (g/dL)	Starting Dialysate Albumin (g/dL)
1 (F6HPS, Qb = 180 mL/min, Qd = 90 mL/min)	15.37 ± 3.06	2.24 ± 0.37	1.77 ± 0.41
2 (F3, Qb = Qd = 150 mL/min)	18.81 ± 2.84	1.90 ± 0.07	1.94 ± 0.23
3 (F3, Qb = 150 mL/min, Qd = 20 mL/min)	16.76 ± 2.35	2.13 ± 0.12	2.29 ± 0.13
4 (F3, Qb = 150 mL/min, Qd = 800 mL/min)	18.28 ± 0.43	2.03 ± 0.02	2.10 ± 0.04
5 (F3, Qb = 150 mL/min, Qd = 2 mL/min)	17.36 ± 1.94	2.15 ± 0.22	2.21 ± 0.14

Table 7: Average Initial Bilirubin and Albumin Concentration. N = 3 for all conditions. Values are shown as mean ± standard deviation.

3.3 kA and kB Parameter Sweep:

The optimal values of kB,BSA and koA for bilirubin removal Setup 1 were found to be kB,BSA = 0.5E7 (1/M) and koA = 2500 mL/min. This result was not sensitive to changing the

number of fibers from n = 8400 provided by Fresenius to n = 9200 from the work of Eloot et al (50). The results are shown in Figure 3. Panel A shows the parameter sweep results for the sum of squares criterion. Panel B shows the parameter sweep results for the percent error criterion. Figure 4 shows the model prediction compared to the true measurements.

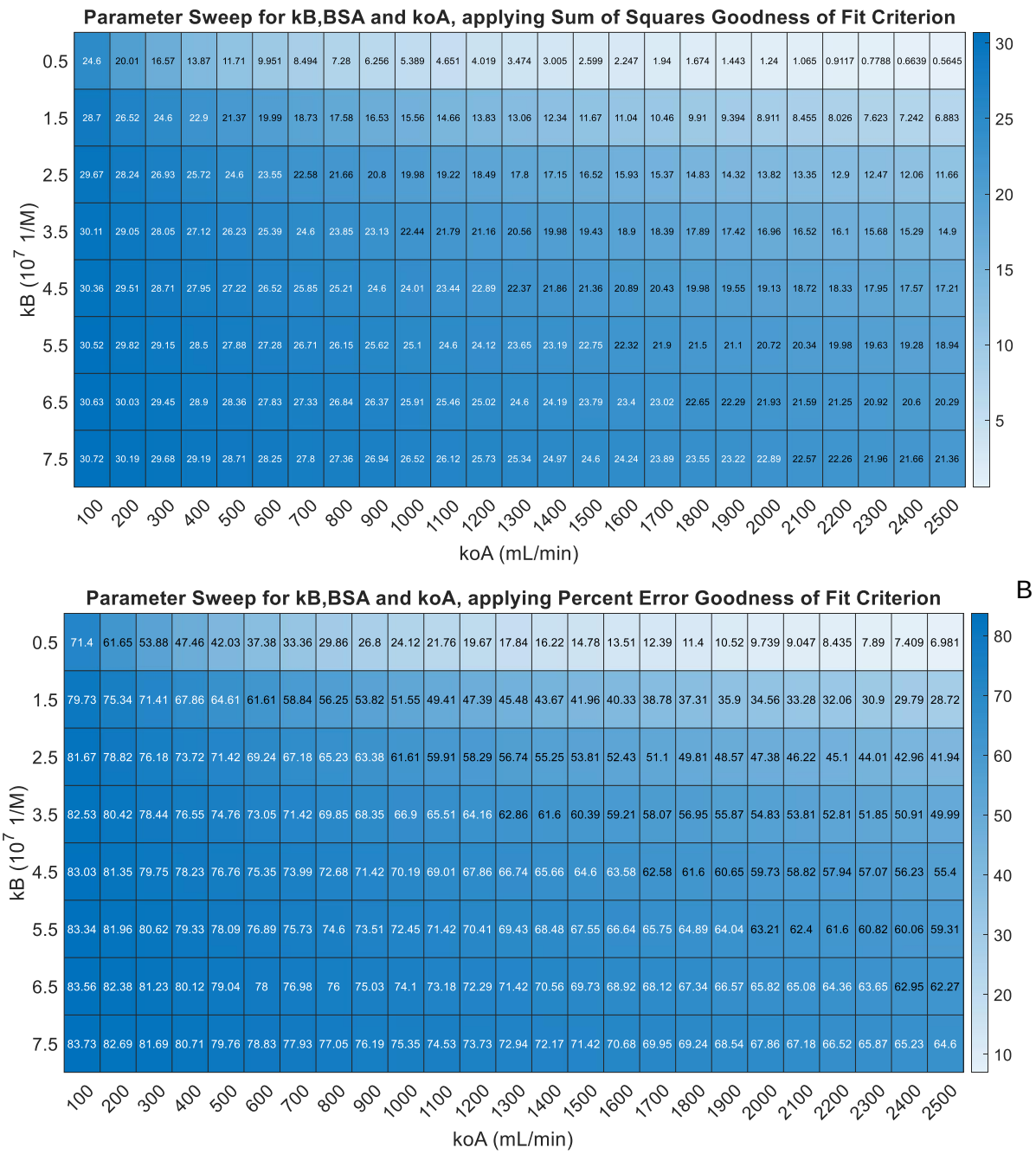

Figure 3: A: Parameter sweep results for kB,BSA for bilirubin and koA, measuring best fit by the sum of squares criterion. B: Parameter sweep results for kB,BSA for bilirubin and koA, measuring best fit by the percent error criterion.

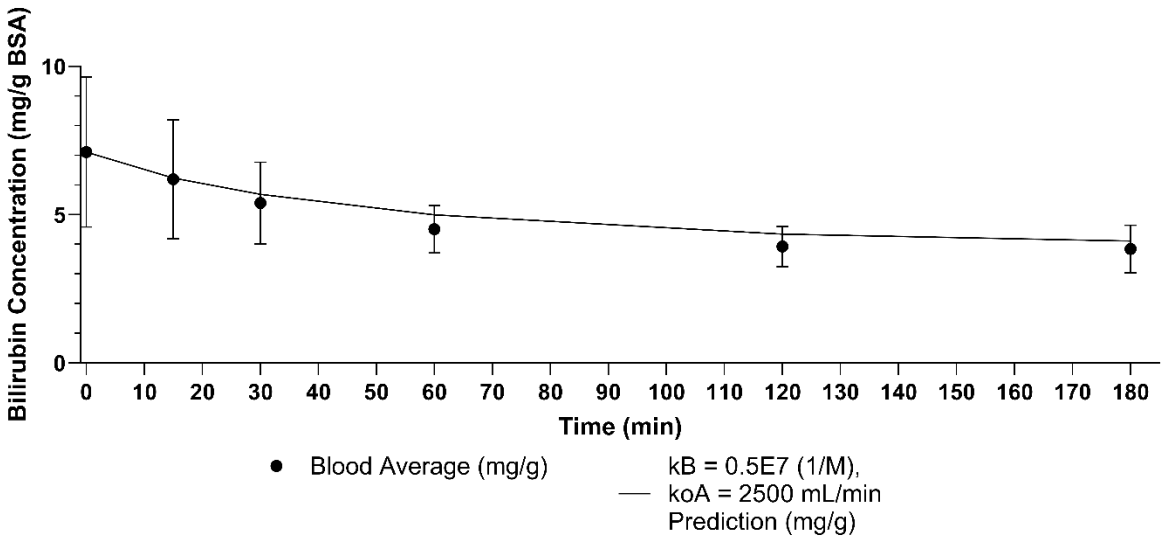

Figure 4: Blood side reservoir bilirubin over time for F6HPS with kB = 0.5E7 (1/M) and koA = 2500 mL/min and n = 8400 compared to experimental data. Error bars are standard deviation. Final percent error 6.98%. Sum of squares error 0.56.

3.4 Model Validation for F3 Dialyzer and Flow Rates

Next, we validated the model using Condition 2, then tested it against the other three flow rates for the F3 polysulfone dialyzer. Applying Equation 20, the new koA for this dialyzer was 770 mL/min. The results of the simulation and experiments are summarized in Figure 5. Experimental results are summarized in Figure 6. Individual conditions are shown in Figure 7.

Figure 5 shows the model predictions for flow rates ranging from 800 mL/min to 1.5 mL/min with a starting bilirubin concentration of 20 mg/dL and starting albumin concentrations on the blood and dialysate side of 2 g/dL. Figure 6 summarizes the % error of the final concentration for all flow rates. Figure 7 shows results for individual conditions and how they compare to model predictions. Table 8 summarizes the accuracy of the model in predicting the outcomes in these conditions. For all flow rates measured except 2 mL/min, the model predicted the final blood bilirubin concentration within 7%.

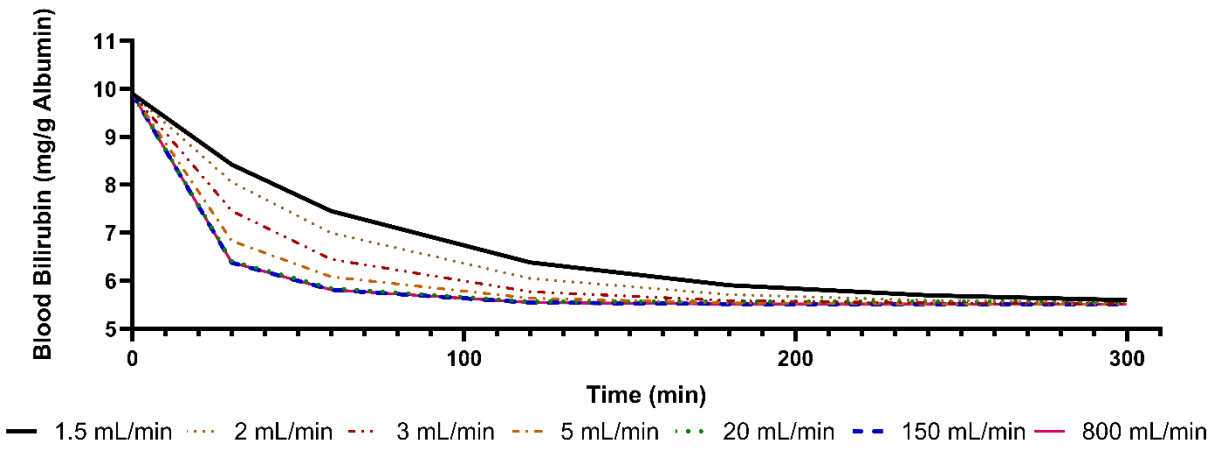

Figure 5: Model predictions for bilirubin removal with an initial blood side bilirubin concentration of 20 mg/dL, and blood and dialysate side BSA concentrations of 2 g/dL.

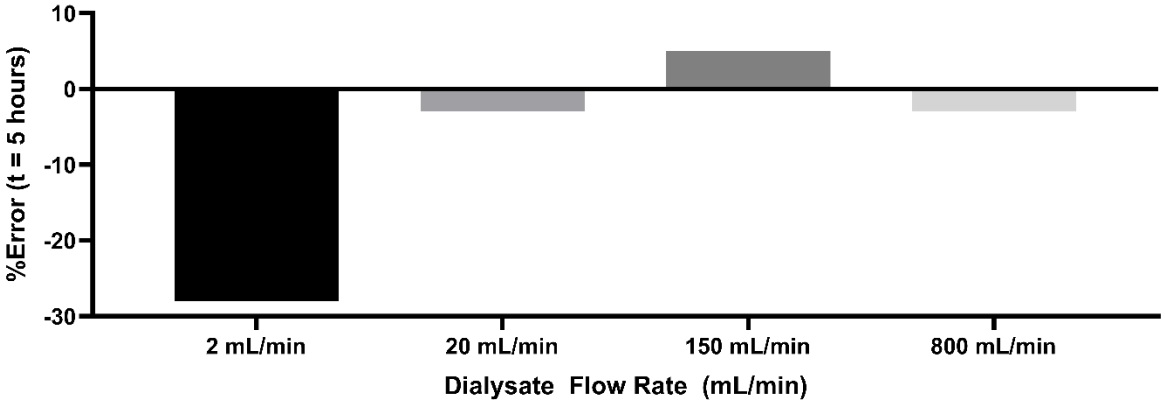

Figure 6: Errors for final bilirubin concentration for F3 dialyzer setup with various flow rates. Numerical values given in Table 8.

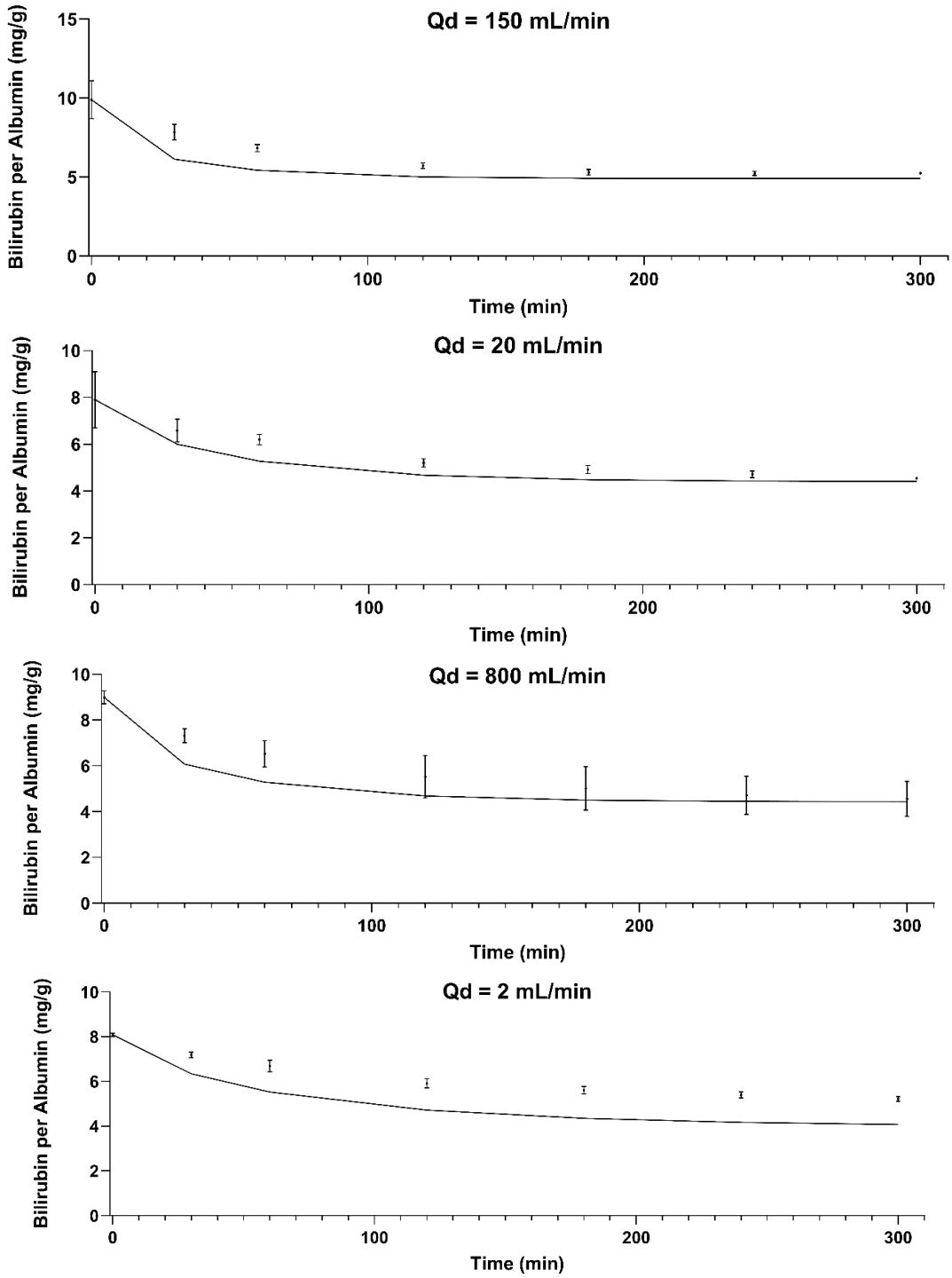

Figure 7: Results and model predictions for dialysate flow rates of 150 mL/min (Panel A), 20 mL/min (Panel B), 800 mL/min (Panel C), and 2 mL/min (Panel D). Errors bars are standard deviation. Where error bars are not shown, it is because they would be smaller than the data point depicted on the graph. Points are experimental data and the line is the model prediction.

Condition	Sum of Squares	Percent Error of Final Value
1 (F6HPS, Qb = 180 mL/min, Qd = 90 mL/min, training)	0.19	6.98%
2 (F3, Qb = Qd = 150 mL/min, validation)	5.74	6.62%
3 (F3, Qb = 150 mL/min, Qd = 20 mL/min, test)	1.77	2.94%
4 (F3, Qb = 150 mL/min, Qd = 800 mL/min, test)	4.14	2.91%
5 (F3, Qb = 150 mL/min, Qd = 2 mL/min, test)	7.89	28%

Table 8: Goodness of Fit for Different Conditions by Sum of Squares and Percent Error of Final Value Criteria.

4 Discussion

This work validates a thermodynamically-based computational model that can be used to rationally design albumin dialysis. This paves the way for optimization of an albumin dialysis system for protein bound toxin removal. It also creates the potential for personalized dialysis regiments, where patients are given flow rate conditions and dialysate compositions tailored to their body volume and toxin concentrations. This would play a similar role to the NxStage Dosing Calculator in home dialysis (66). This work will guide us in optimizing AMOR treatment prescriptions.

This work only analyzed the model's ability to predict the impact of changes in dialyzer and dialysate flow rate. Further work is in progress to predict the impact of changes in blood flow rate and other parameters. Another limitation was small scale. In the test conditions used to validate the model, blood volume was 200 mL – 630 mL. In a patient the plasma volume is approximately 3 L (67). A larger scale *in vitro* test is needed to validate the model's predictive ability in patients.

The model correctly predicts the equilibrium outcomes of albumin dialysis, but it overestimates the kinetics of bilirubin transport across the membrane. This appears mathematically in an implausibly high $K_{free}A$ value. For example, it predicts a $K_{free}A$ value for bilirubin of 2500 mL/min for the F6HPS dialyzer, whose kA for urea is only 746 mL/min under similar flow conditions (68). Pei and colleagues previously reported a bilirubin kA value of 800 mL/min for a Gambro 6LR dialyzer using a similar model (18). The KoA for urea for the Gambro 6LR dialyzer is 736 mL/min (69). We could not replicate their result with a 800 mL/min KoA using their model. A higher KoA value would be needed. In their original work on protein bound toxin removal modeling, Patzer and Bane noted that the dialyzer mass transfer coefficient of their membranes increased after 180 minutes (3 hours) of dialysis (5). They suggested that bilirubin and albumin binding to membrane pores accounts for this phenomenon. It would be very useful to accurately predict bilirubin kinetics in our model so that it can be coupled with models of bilirubin absorption onto activated charcoal to predict the behavior of a combined

dialysis/absorption system like MARS. Thus, we will extend the model to incorporate bilirubin binding to albumin absorbed onto the dialysis membrane.

5 Acknowledgements:

This work was facilitated through the use of advanced computational, storage, and networking infrastructure provided by the Hyak supercomputer system and funded by the STF at the University of Washington.

Alexander Novokhodko acknowledges funding from the National Science Foundation Graduate Research Fellowship Program under Grant No. DGE-1762114. Any opinions, findings, and conclusions or recommendations expressed in this material are those of the author(s) and do not necessarily reflect the views of the National Science Foundation. Alexander Novokhodko acknowledges funding from the Dempsey Startup Competition, Hollomon Health Innovation Challenge, and the Ron and Wanda Crockett Endowed Fellowship in Mechanical Engineering.

6 Bibliography

1. Naghavi M, Ong KL, Aali A, Ababneh HS, Abate YH, Abbafati C, et al. Global burden of 288 causes of death and life expectancy decomposition in 204 countries and territories and 811 subnational locations, 1990–2021: a systematic analysis for the Global Burden of Disease Study 2021. The Lancet. 2024 May;403(10440):2100–32.

2. Lakovic K, Ai J, D'Abbondanza J, Tariq A, Sabri M, Alarfaj AK, et al. Bilirubin and its Oxidation Products Damage Brain White Matter. J Cereb Blood Flow Metab. 2014 Nov;34(11):1837–47.

3. Kalakonda A, Jenkins BA, John S. Physiology, Bilirubin. In: StatPearls [Internet]. Treasure Island (FL): StatPearls Publishing; 2024 [cited 2024 Mar 12]. Available from: http://www.ncbi.nlm.nih.gov/books/NBK470290/

4. Patzer J. Principles of Bound Solute Dialysis. Ther Apher Dial. 2006 Apr;10(2):118–24.

5. Patzer JF, Bane SE. Bound Solute Dialysis. ASAIO J. 2003 May;49(3):271–81.

6. Patzer JF, Safta SA, Miller RH. Slow Continuous Ultrafiltration with Bound Solute Dialysis. ASAIO J. 2006 Jan;52(1):47–58.

7. Padmanabhan A, Connelly-Smith L, Aqui N, Balogun RA, Klingel R, Meyer E, et al. Guidelines on the Use of Therapeutic Apheresis in Clinical Practice – Evidence-Based Approach from the Writing Committee of the American Society for Apheresis: The Eighth Special Issue. J Clin Apheresis. 2019 Jun;34(3):171–354.

8. Magosso E, Ursino M, Colì L, Baraldi O, Bolondi L, Stefoni S. A Modeling Study of Bilirubin Kinetics During Molecular Adsorbent Recirculating System Sessions. Artif Organs. 2006 Apr;30(4):285–300.

9. Annesini MC, Piemonte V, Turchetti L. ALBUMIN-BOUND TOXIN REMOVAL IN LIVER SUPPORT DEVICES: CASE STUDY OF BILIRUBIN ADSORPTION AND DIALYSIS. In:

Biochemical Engineering. New York: Nova Science Publishers; 2009. p. 321–39. (Bioetchnology in Agriculture, Industry and Medicine Series).

10. Annesini MC, Piemonte V, Turchetti L. Artificial liver devices: A chemical engineering analysis. Asia-Pac J Chem Eng. 2011 Jul;6(4):639–48.

11. Annesni MC, Piemonte V, Turchetti L. Artificial liver support systems: a patient-device model. Asia-Pac J Chem Eng. 2014 May;9(3):390–400.

12. Fanali G, di Masi A, Trezza V, Marino M, Fasano M, Ascenzi P. Human serum albumin: From bench to bedside. Mol Aspects Med. 2012 Jun;33(3):209–90.

13. Bai Z, Guo X, Tacke F, Li Y, Li H, Qi X. Association of serum albumin level with incidence and mortality of overt hepatic encephalopathy in cirrhosis during hospitalization. Ther Adv Gastroenterol. 2019 Jan;12:175628481988130.

14. PubChem Compound Summary for CID 5280352, Bilirubin [Internet]. National Center for Biotechnology Information; 2022. Available from: https://pubchem.ncbi.nlm.nih.gov/compound/Bilirubin

15. Yingying Pei, Yize Sun, Yang Xu, Gang Zhao, Dayong Gao, Weiping Ding. A theoretical ultrafiltration model for albumin-bound toxin dialysis. In: 2013 ICME International Conference on Complex Medical Engineering [Internet]. Beijing: IEEE; 2013 [cited 2021 Oct 18]. p. 528–31. Available from: http://ieeexplore.ieee.org/document/6548306/

16. Pei YY, Xu Y, Sun YZ, Gao DY, Ding WP. Numerical Simulation and Experimental Validation of Bound Solute Dialysis in Artificial Liver Support Systems. Adv Mater Res. 2014 Jun;971–973:107–10.

17. Pei YY, Sun YZ, Sun SJ, Gao DY, Ding WP. The Comparison of Albumin Dialysis between Open- and Closed-Loop Dialysis Modes. Adv Mater Res. 2014 Jun;960–961:47–51.

18. Pei Y, Sun Y, Sun S, Gao D, Ding W. Albumin Dialysis in Artificial Liver Support Systems: Open-Loop or Closed-Loop Dialysis Mode? ASAIO J. 2015;61(3):324–31.

19. Villarroel F, Klein E, Holland F. SOLUTE FLUX IN HEMODIALYSIS AND HEMOFILTRATION MEMBRANES: ASAIO J. 1977;23(1):225–32.

20. Liver Support Systems. In: Method of Lines PDE Analysis in Biomedical Science and Engineering [Internet]. Hoboken, NJ, USA: John Wiley & Sons, Inc; 2016 [cited 2022 Sep 16]. p. 165–204. Available from: https://onlinelibrary.wiley.com/doi/10.1002/9781119130499.ch6

21. Saliba F, Camus C, Durand F, Mathurin P, Letierce A, Delafosse B, et al. Albumin Dialysis With a Noncell Artificial Liver Support Device in Patients With Acute Liver Failure: A Randomized, Controlled Trial. Ann Intern Med. 2013 Oct 15;159(8):522.

22. Bañares R, Nevens F, Larsen FS, Jalan R, Albillos A, Dollinger M, et al. Extracorporeal albumin dialysis with the molecular adsorbent recirculating system in acute-on-chronic liver failure: The RELIEF trial. Hepatology. 2013 Mar;57(3):1153–62.

23. Ahmad S, Novokhodko A, Liou IW, Smith NC, Carithers RL, Reyes J, et al. Development and First Clinical Use of an Extracorporeal Artificial Multiorgan System in Acute-on-Chronic Liver Failure Patients. ASAIO J Am Soc Artif Intern Organs 1992. 2024 Feb 29;

24. Stange J, Sponholz C, Kortgen A, Schmidt HHJ, Dollinger M, Hassanein TI. Open albumin dialysis (OPAL) using new micro-structured charcoal adsorbents is significantly more effective in removing toxins and improving related complications of Aoclf than MARS-a multicenter trial. Hepatology. 2018 Oct;68(S1):180A.

25. Marangoni R, Bellati G, Castelli A, Romagnoli E. Development of High-Efficiency Molecular Adsorbent Recirculating System: Preliminary Report. Artif Organs. 2014 Oct;38(10):879–83.

26. Bezanson J, Edelman A, Karpinski S, Shah VB. Julia: A Fresh Approach to Numerical Computing. SIAM Rev. 2017 Jan;59(1):65–98.

27. Rackauckas C, Nie Q. DifferentialEquations.jl – A Performant and Feature-Rich Ecosystem for Solving Differential Equations in Julia. J Open Res Softw. 2017 May 25;5(1):15.

28. Christopher Rackauckas, Avik Pal, Yash Raj Singh, Simon Carlson, Axel Larsson, Qingyu Qu, et al. SciML/NonlinearSolve.jl: v3.1.1 [Internet]. [object Object]; 2023 [cited 2024 Mar 12]. Available from: https://zenodo.org/doi/10.5281/zenodo.10397607

29. Mogensen PK, Carlsson K, Villemot S, Lyon S, Gomez M, Rackauckas C, et al. JuliaNLSolvers/NLsolve.jl: v4.5.1 [Internet]. [object Object]; 2020 [cited 2024 Mar 12]. Available from: https://zenodo.org/record/4404703

30. Verzani J. Root finding functions for Julia} [Internet]. 2020. Available from: https://github.com/JuliaMath/Roots.jl

31. Bieler J. linspace [Internet]. 2020. Available from: https://discourse.julialang.org/t/tl-dr-tips-for-julia-users-coming-from-matlab/41093/1

32. Franco M. remove [Internet]. 2019. Available from: https://stackoverflow.com/questions/35298809/delete-element-in-an-array-for-julia

33. myfind [Internet]. 2017. Available from: https://stackoverflow.com/questions/42232411/find-indices-of-non-zero-elements-from-1-2-0-0-4-0-in-julia-and-create-an-arrr

34. Hairer E, Wanner G. Stiff differential equations solved by Radau methods. J Comput Appl Math. 1999 Nov;111(1–2):93–111.

35. Rackauckas C, Nie Q. Confederated modular differential equation APIs for accelerated algorithm development and benchmarking. Adv Eng Softw. 2019 Jun;132:1–6.

36. Novokhodko A, Gao D, Ahmad S. COMPUTATIONAL MODEL OF SORBENT DIALYSIS. Seattle, WA; IP: 50020.01US1.

37. Leypoldt JK, Cheung AK, Agodoa LY, Daugirdas JT, Greene T, Keshaviah PR, et al. Hemodialyzer mass transfer-area coefficients for urea increase at high dialysate flow rates. Kidney Int. 1997 Jun;51(6):2013–7.

38. Battista J, De Luca D, Eleni Dit Trolli S, Allard L, Bacchetta J, Bouhamri N, et al. CARPEDIEM® for continuous kidney replacement therapy in neonates and small infants: a French multicenter retrospective study. Pediatr Nephrol. 2023 Aug;38(8):2827–37.

39. Noh US, Yi JH, Han SW, Kim HJ. Varying Dialysate Bicarbonate Concentrations in Maintenance Hemodialysis Patients Affect Post-dialysis Alkalosis but not Pre-dialysis Acidosis. Electrolyte Blood Press. 2007;5(2):95.

40. Marano M, Marano S, Gennari FJ. Beyond bicarbonate: complete acid–base assessment in patients receiving intermittent hemodialysis. Nephrol Dial Transplant. 2016 Mar 21;gfw022.

41. Cheung AK, Agodoa LY, Daugirdas JT, Depner TA, Gotch FA, Greene T, et al. Effects of Hemodialyzer Reuse on Clearances of Urea and β_2-Microglobulin. J Am Soc Nephrol. 1999 Jan;10(1):117–27.

42. Leypoldt JK. Methods and Complications of Dialyzer Reuse. In: Handbook of Dialysis Therapy [Internet]. Elsevier; 2008 [cited 2021 Dec 29]. p. 469–77. Available from: https://linkinghub.elsevier.com/retrieve/pii/B9781416041979500363

43. Ding, Weiping. Development of an Optimal Artificial Liver Support System. 1st ed. Seattle: University of Washington; 2010. (PhD Thesis).

44. Senf R, Klingel R, Kurz S, Tullius S, Sauer I, Frei U, et al. Bilirubin-Adsorption in 23 Critically Ill Patients with Liver Failure. Int J Artif Organs. 2004 Aug;27(8):717–22.

45. Lewis B, Panveliwalla D, Tabaqchali S, Wootton IDP. SERUM-BILE-ACIDS IN THE STAGNANT-LOOP SYNDROME. The Lancet. 1969 Feb;293(7588):219–20.

46. ul Amin N, Mahmood R, Asad MJ, Zafar M, Raja A. Evaluating Urea and Creatinine Levels in Chronic Renal Failure Pre and Post Dialysis: A Prospective Study. J Cardiovasc Dis. 2014 Jul;2(4):182–5.

47. Barreto FC, Barreto DV, Liabeuf S, Meert N, Glorieux G, Temmar M, et al. Serum Indoxyl Sulfate Is Associated with Vascular Disease and Mortality in Chronic Kidney Disease Patients. Clin J Am Soc Nephrol. 2009 Oct;4(10):1551–8.

48. Rahelić D, Kujundzić M, Romić Z, Brkić K, Petrovecki M. Serum concentration of zinc, copper, manganese and magnesium in patients with liver cirrhosis. Coll Antropol. 2006 Sep;30(3):523–8.

49. Fresenius Medical Care Renal Therapies Group Personal Communication. 2022.

50. Eloot S, Vos JY, Vos F, Hombrouckx R, Verdonck P. Middle molecule removal in low-flux polysulfone dialyzers: Impact of flows and surface area on whole-body and dialyzer clearances. Hemodial Int. 2005 Oct;9(4):399–408.

51. Dukhin SS, Tabani Y, Lai R, Labib OA, Zydney AL, Labib ME. Outside-in hemofiltration for prolonged operation without clogging. J Membr Sci. 2014 Aug;464:173–8.

52. Bieber S, Halldorson JB, Finn E, Ahmad S, Chamberlain JS, Odom GL. Extracorporeal Delivery of rAAV with Metabolic Exchange and Oxygenation. Sci Rep. 2013 Dec;3(1):1538.

53. Sangeetha MS, Kandaswamy A, Lakshmi Deepika C, Revanth CV. FINITE ELEMENT ANALYSIS FOR COMPARING THE PERFORMANCE OF STRAIGHT AND UNDULATED FIBERS IN ALTERING THE FILTERING EFFICIENCY OF HEMODIALYZER MEMBRANES. J Mech Med Biol. 2019 Aug;19(05):1850063.

54. Liao Z, Klein E, Poh C, Huang Z, Lu J, Hardy P, et al. Measurement of hollow fiber membrane transport properties in hemodialyzers. J Membr Sci. 2005 Apr 7;S0376738805001602.

55. Chen RF. The Fluorescence of Bilirubin-Albumin Complexes. In: Thaer AA, Sernetz M, editors. Fluorescence Techniques in Cell Biology [Internet]. Berlin, Heidelberg: Springer Berlin Heidelberg; 1973 [cited 2022 Sep 19]. p. 273–82. Available from: http://link.springer.com/10.1007/978-3-642-49204-4_27

56. Faerch T, Jacobsen J. Determination of association and dissociation rate constants for bilirubin-bovine serum albumin. Arch Biochem Biophys. 1975 Jun;168(2):351–7.

57. Rubaltelli FF, Jori G. VISIBLE LIGHT IRRADIATION OF HUMAN AND BOVINE SERUM ALBUMIN-BILIRUBIN COMPLEX*. Photochem Photobiol. 1979 May;29(5):991–1000.

58. Mir MM, Majid Fazili K, Abul Qasim M. Chemical modification of buried lysine residues of bovine serum albumin and its influence on protein conformation and bilirubin binding. Biochim Biophys Acta BBA - Protein Struct Mol Enzymol. 1992 Mar;1119(3):261–7.

59. Williams KR, Adhyaru B, Pierce RE, Schulman SG. The Binding Constant for Complexation of Bilirubin to Bovine Serum Albumin. An Experiment for the Biophysical Chemistry Laboratory. J Chem Educ. 2002 Jan;79(1):115.

60. Chen J, Song G, He Y, Yan Q. Spectroscopic analysis of the interaction between bilirubin and bovine serum albumin. Microchim Acta. 2007 Jun;159(1–2):79–85.

61. Meyer TW, Peattie JWT, Miller JD, Dinh DC, Recht NS, Walther JL, et al. Increasing the Clearance of Protein-Bound Solutes by Addition of a Sorbent to the Dialysate. J Am Soc Nephrol. 2007 Mar;18(3):868–74.

62. Michaels AS. Operating parameters and performance criteria for hemodialyzers and other membrane-separation devices. Trans - Am Soc Artif Intern Organs. 1966;12:387–92.

63. Peng Z, Yang Y, Luo J, Nie C, Ma L, Cheng C, et al. Nanofibrous polymeric beads from aramid fibers for efficient bilirubin removal. Biomater Sci. 2016;4(9):1392–401.

64. Ouseph R, Ward RA. Increasing Dialysate Flow Rate Increases Dialyzer Urea Mass Transfer-Area Coefficients During Clinical Use. Am J Kidney Dis. 2001 Feb;37(2):316–20.

65. Benavente J. Electrokinetic characterization of composite membranes: estimation of different electrical contributions in pressure induced potential measured across reverse osmosis membranes. J Membr Sci. 2000 Jul 1;172(1–2):189–97.

66. Molina P, Gonzalez-Moya M, Vizcaıno B, Beltran S, Molina M, Sanchis I, et al. RELATIONSHIP BETWEEN PREDICTIVE KT/V AND CALCULATED KT/V ACHIEVED WITH NXSTAGE CYCLER IN SHORT-DAILY HOME HEMODIALYSIS PATIENTS. Nephrol Dial Transplant. 2018 May 1;33(suppl_1):i505–6.

67. Sharma R, Sharma S. Physiology, Blood Volume. In: StatPearls [Internet]. Treasure Island (FL): StatPearls Publishing; 2024 [cited 2024 Apr 23]. Available from: http://www.ncbi.nlm.nih.gov/books/NBK526077/

68. Li PKT, Cheng YL, Leung CB, Szeto CC, Chow KM, Kwan BCH, et al. Effect of Membrane Permeability on Inflammation and Arterial Stiffness: A Randomized Trial. Clin J Am Soc Nephrol. 2010 Apr;5(4):652–8.

69. Ahmad S, Misra M, Hoenich N, Daugirdas JT. Equipo de hemodiálisis. In: Manual de Diálisis. 5th ed. Barcelona: Wolters Kluwer; 2015.